Solving the Grad-Shafranov Equation with Spectral Elements

E.C. Howell[a,1,], C.R. Sovinec[a]

[a]*University of Wisconsin-Madison, Department of Engineering Physics, Engineering Research Building, 1500 Engineering Dr, Madison, Wi, USA, 53706*

Abstract

The development of a generalized two dimensional MHD equilibrium solver within the NIMROD framework [1] is discussed. Spectral elements are used to represent the poloidal plane. To permit the generation of spheromak and other compact equilibria, special consideration is given to ensure regularity at the geometric axis. The scalar field $\Lambda = \psi/R^2$ is used as the dependent variable to express the Grad-Shafranov operator as a total divergence. With the correct gauge, regularity along the geometric axis is satisfied. The convergence properties of the spectral elements are investigated by comparing numerically generated equilibria against known analytic solutions. Equilibria accurate to double precision error are generated with sufficient resolution. Depending on the equilibrium, either geometric or algebraic convergence is observed as the polynomial degree of the spectral-element basis is increased.

Keywords: Grad-Shafranov, Magnetohydrodynamic Equilibrium, Compact Torus, Spectral Element

1. Introduction

The analysis of magnetohydrodynamic (MHD) equilibrium is central to the study of macroscopic dynamics in magnetically confined plasmas. Equilibria are the starting point for many transport and stability calculations. The ex-

Email addresses: `ehowell@wisc.edu` (E.C. Howell), `csovinec@cae.wisc.edu` (C.R. Sovinec)

treme anisotropy and disparity in characteristic spatial scales associated with these calculations requires accurate numerical methods and accurate equilibrium profiles. High-order and spectral-elements have proven to be effective methods for these calculations [1], but numerical errors generated when importing externally calculated equilibria tend to get amplified by high-order stability computations. NIMEQ [2], a general purpose Grad-Shafranov equilibrium solver, has been developed for the NIMROD code using NIMROD'S spectral element representation. Using the same representation for equilibrium and for stability eliminates interpolation errors. The spectral-element representation also allows for the generation of high-quality equilibria on moderately sized meshes.

Magnetostatic equilibria are described by the force balance equation, the magnetic divergence constraint, and Ampere's law:

$$\vec{J} \times \vec{B} = \nabla P \tag{1}$$

$$\nabla \cdot \vec{B} = 0 \tag{2}$$

$$\nabla \times \vec{B} = \mu_0 \vec{J} \tag{3}$$

where $\vec{J}$ is the current density, $\vec{B}$ is the magnetic field, P is the plasma pressure, and μ_0 is the permeability of free space.

For conditions of axisymmetry, the magnetic field is expressed as $\vec{B} = \nabla\phi \times \nabla\psi + F\nabla\phi$ in the cylindrical coordinate system (R, Z, ϕ). The flux function ψ is related to the physical poloidal flux, divided by a factor of 2π. A similar representation for the current is found using Ampere's law $\mu_0\vec{J} = \mu_0 R J_\phi \nabla\phi + \nabla F \times \nabla\phi$.

From Equation 1 it is observed that $\vec{B} \cdot \nabla P = 0$, implying that the pressure is a flux function $P = P(\psi)$. Similarly, $\vec{J} \cdot \nabla P = 0$, and $F(\psi) = RB_\phi$ is also a flux function. Inserting the above definitions for $\vec{B}$ and $\vec{J}$ into Equation 1 yields the Grad-Shafranov equation [3, 4]:

$$\Delta^*\psi = -\mu_0 R^2 \frac{dP}{d\psi} - F(\psi)\frac{dF}{d\psi}, \tag{4}$$

where the Grad-Shafranov operator is defined as

$$\Delta^* \equiv R\frac{\partial}{\partial R}R^{-1}\frac{\partial}{\partial R} + \frac{\partial^2}{\partial Z^2}.$$

(5)

Equation 4 is a second order nonlinear elliptic equation describing axis-symmetric plasma equilibria in toroidal geometry. The two free functions $P(\psi)$ and $F(\psi)$ are either prescribed or determined from transport effects (not considered here).

Analytic solutions to the Grad-Shafranov equation have been found for simple prescriptions of $F(\psi)$ and $P(\psi)$[5–9]. These solutions have limited applicability to most plasma experiments, and numerical solutions are often needed. Numerical techniques for solving the Grad-Shafranov equation are categorized according to the specification of the flux along the boundary and by the choice of independent variables. Fixed-boundary solvers specify the flux function along the boundary. Free-boundary solvers self-consistently calculate the boundary flux from external magnetic coils and internal plasma currents. Direct solvers calculate the flux on a physical (R, Z) mesh. Indirect solvers specify a flux-based mesh and calculate the physical coordinates $R(\psi, \theta)$ and $Z(\psi, \theta)$ as functions of ψ and a poloidal angle θ. The Grad-Shafranov equation has been solved using finite difference [10], spectral methods [11], Green's functions [12], linear finite elements [13, 14], and Hermite cubic finite elements [15]. Many of these methods are designed for topologically toroidal systems and do not address the regularity issues associated with the R^{-1} factor appearing in Equation 4 in cylindrical domains. A few codes have been specifically modified to treat compact devices that are topologically cylindrical, including consideration of current on open magnetic field lines [16].

The second section of this letter develops the algorithm used by NIMEQ, a fixed-boundary direct Grad-Shafranov solver. A 2-D spectral element mesh is used to represent the poloidal plane. Special consideration is given to ensure proper regularity at the geometric axis. The derivation presented uses a cylindrical coordinate system, but the code is generalized to also work in linear coordinates. Benchmarking and convergence studies are presented in the third section, where equilibria with known and unknown analytic solutions are

3

considered. A discussion and conclusions are presented in the last section.

2. Numerical Algorithm

This section presents the Galerkin formulation used to solve the Grad-Shafranov equation in weak form. Substituting the scalar field $\Lambda = \psi/R^2$ into Equation 4 transforms the Grad-Shafranov operator into a divergence of a vector, $\Delta^*\psi = \nabla \cdot R^2\nabla\Lambda$. This is convenient for topologically cylindrical domains, because all surface terms that arise are at physical boundaries and not along $R = 0$. The field Λ is then spilt into a known component Λ_0 and an unknown component Λ_h. Λ_0 satisfies the specified inhomogeneous boundary condition for Λ, and Λ_h satisfies the boundary condition $\Lambda_h = 0$. The unknown field is expanded onto a series of spectral element basis functions, $\Lambda_h = \sum_i \Lambda_i\alpha_i$, where α_i are the bases of two-dimensional nodal elements with nodes located according to Gauss-Lobatto-Legendre integration [17]. Substituting this expression for Λ into Equation 4, multiplying the equation by the test function α_j, and integrating over the domain yields the following weak form of the Grad-Shafranov equation:

$$\sum_i \Lambda_i \int dV\, R^2\nabla\alpha_i \cdot \nabla\alpha_j = \int dV (FF' + \mu_0 R^2 P')\alpha_j - \int dV\, R^2\nabla\Lambda_0 \cdot \nabla\alpha_j. \quad (6)$$

In NIMEQ, the integrals are performed by Gaussian integration, and isoparametric mapping is used to model a variety of domain shapes.

The above expression holds for all test functions α_j, defining an algebraic system. For compactness Equation 6 is written as $M\Lambda = Q$. The matrix M in positive definite and symmetric. In general, the right-hand-side vector Q is nonlinear, due to the $P(\psi)$ and $F(\psi)$ functions. In our applications so far, using modified Picard iterations,

$$M\Lambda^n = (1 - \theta) M\Lambda^{n-1} + \theta Q^{n-1}, \quad (7)$$

has been satisfactory, where the relaxation parameter $\theta \in (0, 1]$ is introduced to aid convergence. The matrix in Equation 7 is inverted using standard numerical

4

techniques. Convergence is achieved when the ratio of the norms of the residual error, $\|\Delta^*\psi + FF' + \mu_0 R^2 P'\|_2$, and del-star operation $\|\Delta^*\psi\|_2$ is less than a user-specified tolerance.

A normalized "ring" flux $\hat{\psi} = (\psi - \psi_a) / (\psi_l - \psi_a)$ is defined to help constrain the physical region over which different $P(\psi)$ and $F(\psi)$ profiles are applied. The normalized flux is defined to be 0 at the magnetic axis ψ_a, and 1 at the last closed-flux surface ψ_l. The last closed flux surface is assumed to be the extreme value of the flux on the boundary. The normalized flux also serves as a marker to distinguish between regions of open and closed flux. This enables the tailoring of $P(\psi)$ and $F(\psi)$ to account for different physical effects that occur in the two regions.

In topologically cylindrical domains, regularity requires the flux function to vary as $\psi(R, Z) = \psi_0 + \psi_2(Z) R^2 + O(R^4)$ in the limit of $R \to 0$. The corresponding behavior for Λ is $\Lambda = \psi_0 / R^2 + \psi_2(Z) + O(R^2)$. A gauge freedom exists in that the magnetic field and the current density only depend on the derivatives of ψ. The choice $\psi_0 = 0$ implies that Λ satisfies standard regularity conditions for an axis-symmetric scalar field and, hence, is well behaved near the geometric axis in our computations.

The final step is to calculate the equilibrium fields from the converged solution for Λ. NIMROD computations require the equilibrium quantities $\vec{B}_p$, $\vec{J}_p$, RB_ϕ, $R^{-1}J_\phi$, and P at each node of the spectral-element expansion. The pressure and RB_ϕ values are calculated directly from the prescribed $P(\psi)$ and $F(\psi)$ profiles using the computed $\Lambda(R, Z)$ field. The poloidal magnetic field is expressed in terms of Λ,

$$\vec{B}_p = R^{-1}\hat{e}_\phi \times \left(2R\hat{e}_r\Lambda + R^2\nabla\Lambda\right), \tag{8}$$

and projected onto the spectral-element bases by solving a mass-matrix. The poloidal current is calculated directly from the poloidal magnetic field using the relation $\mu_0\vec{J}_p = -F'\vec{B}_p$. A mass-matrix inversion is performed to find expansion coefficients of $\mu_0 R^{-1} J_\phi = R^{-2}\Delta^*\psi = \mu_0 P' + R^{-2}FF'$ for the toroidal current density used by NIMROD.

3. Spectral Convergence Studies

This section presents the verification and convergence properties of our spectral element computations. In three of the test cases, the Grad-Shafranov equations is linear in ψ, and analytical solutions are known. These equilibria represent idealizations of a tokamak, a spheromak, and a field-reversed configuration (FRC). The Grad-Shafranov equation is nonlinear in ψ in a fourth case, and analytical solutions are not known.

Convergence studies using both h-refinement and p-refinement are performed for the first three equilibria by comparing numerically generated equilibria with their known solutions. Another measure of convergence is determined by defining a spectral error based on the truncation of the spectral representation. This is done by projecting the solution onto 2D Legendre polynomials within each element. The spectral error is defined as $E_s \equiv \sqrt{\sum_e c_e^2/n^2}$, where c_e is the coefficient of the highest order Legendre polynomial in each element and n is the number of elements. The spectral error gives an estimate of the truncation error (E_T), which results from keeping a finite number of terms in an expansion. As a rule of thumb, the truncation error for a geometrically converging series is $E_T \sim O\left(E_s\right)$, and for an algebraically converging expansion, the error is $E_T \sim O\left(\text{p}E_s\right)$, where p is the degree of the highest-order term in the expansion [17]. The convergence properties of the spectral error is compared with the numerical error for the first three equilibria. The spectral error alone is used to investigate the convergence properties of the nonlinear equilibrium.

3.1. Equilibria

The first test case, representative of a tokamak, is the Solov'ev solution to Equation 4. Solutions are obtained by asserting that both $\mu_0 P' = -S_1$ and $FF' = S_2$ are constant [5]. The resulting equilibrium equation is linear, and series solutions are straightforward to calculate [18, 19]. Here, we use a simple nontrivial case, where the analytic solution is:

$$\psi = -\frac{S_1}{8}R^2 - \frac{S_2}{2}Z^2 + S_3 + S_4R^2 + S_5\left(R^4 - 4R^2Z^2\right). \tag{9}$$

Convergence studies are performed in a domain of rectangular poloidal cross section with $-1.5 < Z < 1.5$ and $1.5 < R < 4.5$. The equilibrium is parameterized using $S_1 = 0.176$, $S_2 = 0.5$, $S_3 = -0.496$, $S_4 = 0.198$ and $S_5 = 0.011$. The poloidal flux along the boundary is prescribed using Equation 9. When analyzing the convergence properties of this equilibrium, it is worth noting that while ψ is a 4-th order polynomial, our dependent variable Λ has terms that are proportional to R^{-2}. Consequently, ψ can be represented exactly by a single 4-th order element but Λ cannot. Thus, the numerical accuracy in Λ and ψ continue to increase as our mesh is refined when using 4-th order or higher elements.

The second test case is a field-reversed configuration (FRC). FRCs are characterized by small or zero toroidal field, so $F = 0$ is prescribed in the Grad-Shafranov computations. A quadratic pressure profile $P = P_0 + P_2 \left(\psi^2/\psi_0^2\right)$ is specified, and the resulting equation for ψ is linear:

$$\Delta^* \psi + 2\mu_0 R^2 P_2 \frac{\psi}{\psi_0^2} = 0. \tag{10}$$

Equation 10 can be solved for a cylinder of height h and radius a with the boundary condition $\psi = 0$. The resulting equilibrium is:

$$\psi = \psi_0 \frac{F_0\left(\eta, \frac{1}{2}\sqrt{d}r^2\right)}{F_0\left(\eta, \frac{1}{2}\sqrt{d}r_0^2\right)} \sin\left(\lambda z\right) \tag{11}$$

$$B_r = -\frac{\lambda}{r}\psi_0 \frac{F_0\left(\eta, \frac{1}{2}\sqrt{d}r^2\right)}{F_0\left(\eta, \frac{1}{2}\sqrt{d}r_0^2\right)} \cos\left(\lambda z\right) \tag{12}$$

$$B_z = \sqrt{d}\psi_0 \frac{F_0'\left(\eta, \frac{1}{2}\sqrt{d}r^2\right)}{F_0\left(\eta, \frac{1}{2}\sqrt{d}r_0^2\right)} \sin\left(\lambda z\right), \tag{13}$$

where F_0 is the 0-th order Coulomb wave function, $d = 2\mu_0 P_2/\psi_0^2$, $\lambda = \pi/h$, and $\eta = \lambda^2/\left(4\sqrt{d}\right)$[6, 7]. The flux at the magnetic axis ψ_0 is determined self-consistently such that the radial boundary condition $F_0\left(\eta, \sqrt{d}a^2/2\right) = 0$ is satisfied.

We calculate the zeros of the Coulomb wave function $F_0(\eta, \rho)$ numerically to ten significant digits using Newton's method. We set the equilibrium parameters to make $\eta = 0.3315$ so that B_r has its first zero at $\rho \equiv \sqrt{d}a^2/2 = 4$. This corresponds to a FRC with elongation $E \equiv a/2h = 0.52$. The domain is a cylinder of height $h = 1.0$ and radius $a = 1.04$. The pressure is set to $\mu_0 P_2 = 0.277$, corresponding to a flux on axis of $\psi = \pm 0.1$. The solution that a numerical algorithm converges on is determined by the initial guess used to seed the nonlinear iterations. In this study NIMEQ converges on the negative root.

The third test case is the ideal spheromak. Under the assumption of constant pressure, the magnetic field is parallel to the current and Ampere's law becomes $\nabla \times \vec{B} = \lambda \vec{B}$. The parallel current, $\lambda = \mu_0 \vec{J} \cdot \vec{B}/B^2$, is related to the flux function $F(\psi)$ by $\lambda = -F'(\psi)$. In a cylinder of height h and radius a, and considering constant λ, the lowest order nontrivial solution is:

$$\psi = \psi_0 \frac{\gamma_{11} r}{\chi_{01}} \frac{J_1(\gamma_{11} r)}{J_1(\chi_{01})} \sin\left(\frac{\pi}{h} z\right) \tag{14}$$

$$B_r = -\psi_0 \frac{\pi}{h} \frac{\gamma_{11}}{\chi_{01}} \frac{J_1(\gamma_{11} r)}{J_1(\chi_{01})} \cos\left(\frac{\pi}{h} z\right) \tag{15}$$

$$B_z = \psi_0 \frac{\gamma_{11}^2}{\chi_{01}} \frac{J_0(\gamma_{11} r)}{J_1(\chi_{01})} \sin\left(\frac{\pi}{h} z\right) \tag{16}$$

$$B_\phi = -\lambda \psi_0 \frac{\gamma_{11}}{\chi_{01}} \frac{J_1(\gamma_{11} r)}{J_1(\chi_{01})} \sin\left(\frac{\pi}{h} z\right). \tag{17}$$

The parallel current satisfies $\lambda^2 = \gamma_{11}^2 + (\pi^2/h^2)$ where $\gamma_{11} = \chi_{11}/a$ and χ_{i1} is the first zero of the Bessel function J_i[9].

A cylindrical spheromak is modeled with height $h = 0.5$ and radius $a = 0.5$, and $\psi = 0$ at the boundary. A uniform pressure profile is used by setting $P' = 0$, and a linear poloidal current function is specified $F = (\hat{\psi} - 1)$. We note that prescribing P and F in terms of the normalized flux $\hat{\psi}$ sets the magnitude of the right side of Equation 4, independent of $|\psi_l - \psi_a|$. Thus, cases such as our FRC and spheromak equilibria, where the right side of Equation 4 is a linear monomial in ψ, have a unique solution, apart from a sign. As noted for the

8

FRC case, the sign of the flux is determined by the seed field used at the start of the iteration. For our spheromak cases, we choose $\lambda\psi_a = 1$.

The fourth case is more representative of applications where the Grad-Shafranov equation is nonlinear in ψ. We specify a quadratic F profile, $F = \left(1 - \hat{\psi}\right) + \hat{\psi}\left(\hat{\psi} - 1\right)/4$ and either a cubic pressure profile, $\mu_0 P = \mu_0 P_a \left(1 - 3\hat{\psi}^2 + 2\hat{\psi}^3\right)$ or a uniform pressure profile. Calculations are performed in a cylinder of height $h = 1$ and radius $a = 0.5$ with $\psi = 0$ on the boundary.

Table 1 summarizes the four different equilibria studied, and the calculated equilibrium fluxes are shown Figure 1.

3.2. Convergence Studies

Convergence studies are performed for the Solev'ev, FRC, spheromak equilibria by comparing the numerical and analytic solutions. The numerical error of a quantity ξ is defined as $E_n \equiv \sqrt{\sum \left(\xi_n - \xi_a\right)^2 / \sum \xi_a^2}$ where ξ_n is the numerical solution and ξ_a is the analytic solution. The summation is performed over all the spectral-element nodes. Convergence studies using h-refinement are performed by increasing the number of elements at a fixed polynomial degree. Here the error for a smooth solution of a second order differential equation is expected to converge as $h^{(p+1)}$, where h is a characteristic element length and p is the polynomial degree. The error in derivatives of the solution are expected to scale as h^P[20].

Our studies are performed using meshes with equal numbers of elements in the radial and vertical directions. H-refinement studies are repeated using elements with polynomial degrees ranging from 2 to 10. The error in ψ is plotted verses the number of elements in the radial direction on a log-log plot for the Solev'ev equilibrium in Figure 2. The error in ψ and B_r is also plotted for the FRC and spheromak equilibria. In all cases, the error decays linearly to a minimum error (discussed below), indicating algebraic convergence. The asymptotic rate of convergence is indicated by the slope of these lines. The toroidal field, RB_ϕ, is calculated directly from ψ, and converges at a similar rate to ψ. Both B_r and B_z are calculated from $\nabla\psi$, and B_z converges at a rate

similar to B_r, but at a reduced rate compared to ψ.

The calculated rates of convergence for ψ are shown in Table 2. For lower-order polynomials the rates of convergence in ψ are between p + 1 and p + 2. With higher-order polynomials, p > 6, the solutions reach accuracies limited by double-precision error before a clear asymptotic range of convergence is observed. It is not apparent as to why the flux converges faster than the predicted p + 1 rate, nor is it clear if the trend continues to higher polynomial degree. The calculated rates of convergence for B_r are given in Table 3 for the FRC and spheromak equilibria. The obtained rates of convergence are close to the expected rate p.

Errors as small as 10^{-14} are achieved for the Solev'ev equilibrium and 10^{-13} for the spheromak equilibrium. The accuracy of these two cases is limited by double precision error. Our reported errors in the FRC cases are as small as 10^{-10}. This minimum is a reflection of the accuracy in computing the analytic solution. Due to the difficulty in calculating zeros of the Coulomb wave function, the reference solution is only available to ten significant digits.

P-refinement convergence studies are performed by increasing the polynomial degree of the elements while keeping the number of elements in a mesh fixed. The numerical error is calculated as before for the Solev'ev, FRC, and spheromak cases. The numerical errors are plotted versus the polynomial degree on a semi-log scale for 2×2 and 8×8 element meshes in Figure 3. The linear nature of the plots indicates geometric convergence[17]. The spectral error in ψ is calculated for these cases and plotted on a semi-log plot versus the polynomial degree in Figure 4. Similar to the numerical error, geometric convergence is observed up to double precision error.

The spectral error for the nonlinear equilibrium with the cubic pressure profile is plotted as a function of polynomial degree in Figures 5A-B. Algebraic convergence is observed as the error is linear on the log-log scale (5B) but not on the log-linear scale (5A). Even with the algebraic convergence, accurate solutions are obtained for the nonlinear equilibrium. For the 8×8 element mesh, the spectral error reaches the double-precession limit of 10^{-16}, using 17-th order

polynomials. Using 20-th order polynomials the 2×2 and 4×4 element meshes have spectral errors of 1.99×10^{-13} and 1.45×10^{-15}, respectively.

Geometric convergence of spectral methods is expected for well behaved solutions. The existence of singularities and branch points can result in algebraic convergence [17]. A second nonlinear equilibrium is studied to test whether the algebraic convergence observed with the cubic pressure profile is due to the behavior of the solution or due to the numerical representation. This second nonlinear equilibrium uses the same geometry and $F(\psi)$ profile as the first. However, the second equilibrium uses a constant $P(\psi)$ instead of the cubic profile. The second case is nonlinear because FF' is cubic in ψ. The spectral error for this equilibrium is shown in Figure 5C. Geometric convergence is obtained with the constant pressure profile, suggesting that the observed algebraic convergence for the first nonlinear equilibrium is due to properties of the solution and not the numerical implementation.

4. Conclusions

A new Grad-Shafranov solver has been implemented using 2-D spectral elements. To our knowledge this is the first code to use spectral elements to solve the Grad-Shafranov equation. Unlike many equilibrium codes designed specifically for tokamaks, NIMEQ accounts for regularity at the geometric axis. This affords us additional generality allowing for the modeling of compact devices in addition to tokamaks and other toroidal configurations. Our spheromak and FRC equilibria contain the geometric axis in their domain and provide tests of regularity. Highly accurate solutions of ψ and $\vec{B}$ with numerical errors on the order 10^{-13} or smaller are obtained. Finally, a spectral error based on the truncation error of the spectral element expansion is described. This error reproduces the same qualitative behavior observed in the numerical error in our first three tests, but it does not require knowledge of the exact solution.

We close by highlighting the power of the spectral element representation over traditional finite elements. Consider the FRC equilibrium, where a 128×128 element mesh with 2nd order polynomial elements produces a numerical

error in ψ of 1.06×10^{-8}. This mesh has approximately $100,000$ degrees of freedom. The numerical error in ψ for a 2×2 mesh with 10-th order elements is 3.83×10^{-9}. This mesh has approximately 500 degrees of freedom.

Acknowledgements

References

[1] C. R. Sovinec, A. H. Glasser, T. A. Gianakon, D. C. Barnes, R. A. Nebel, S. E. Kruger, D. D. Schnack, S. J. Plimpton, A. Tarditi, M. S. Chu, and the NIMROD Team, Nonlinear magnetohydrodynamics simulation using high-order finite elements, J. Comput. Phys. 195 (2004) 355 – 386.

[2] E. C. Howell, C. R. Sovinec, NIMEQ: MHD equilibrium solver for NIM-ROD, Bull. Am. Phys. Soc. vol. 53, No 14, BP6.00041 (2008).

[3] H. Grad, H. Rubin, Hydromagnetic equilibria and force-free fields, in: Proceedings of the Second United Nations Conference on the Peaceful Uses of Atomic Energy, volume 31, United Nations, p. 190.

[4] V. D. Shafranov, On magnetohydrondynamical equilibrium configurations, Soviet Physics JETP-USSR 6 (1958) 545–554.

[5] L. S. Solovev, Theory of hydromagnetic stability of toroidal plasma con-figuartions, Soviet Physics JETP-USSR 26 (1968) 400.

[6] P. B. Parks, M. J. Schaffer, Analytical equilibrium and interchange stability of single- and double-axis field-reversed configurations inside a cylindrical cavity, Phys. Plasmas 10 (2003) 1411–1423.

[7] H. L. Berk, J. H. Hammer, H. Weitzner, Analytic field-reversed equilibria, Phys. Fluids 24 (1981) 1758–1759.

[8] M. Rosenbluth, M. Bussac, MHD stability of spheromak, Nucl. Fusion 19 (1979) 489.

[9] J. M. Finn, W. M. Manheimer, E. Ott, Spheromak tilting instability in cylindrical geometry, Phys. Fluids 24 (1981) 1336–1341.

[10] J. Johnson, H. Dalhed, J. Greene, R. Grimm, Y. Hsieh, S. Jardin, J. Manickam, M. Okabayashi, R. Storer, A. Todd, D. Voss, K. Weimer, Numerical determination of axisymmetric toroidal magnetohydrodynamic equilibria, J. Comput. Phys. 32 (1979) 212 – 234.

[11] K. Ling, S. Jardin, The princeton spectral equilibrium code: PSEC, J. Comput. Phys. 58 (1985) 300 – 335.

[12] L. Lao, H. S. John, R. Stambaugh, A. Kellman, W. Pfeiffer, Reconstruction of current profile parameters and plasma shapes in tokamaks, Nucl. Fusion 25 (1985) 1611.

[13] J. Blum, J. L. Foll, B. Thooris, The self-consistent equilibrium and diffusion code sced, Comput. Phys. Commun. 24 (1981) 235 – 254.

[14] R. Gruber, R. Iacono, F. Troyon, Computation of mhd equilibria by a quasi-inverse finite hybrid element approach, J. Comput. Phys. 73 (1987) 168 – 182.

[15] H. Lutjens, A. Bondeson, A. Roy, Axisymmetric MHD equilibrium solver with bicubic hermite elements, Comput. Phys. Commun. 69 (1992) 287 – 298.

[16] E. Hooper, L. Pearlstein, R. Bulmer, MHD equilibria in a spheromak sustained by coaxial helicity injection, Nucl. Fusion 39 (1999) 863–871.

[17] J. P. Boyd, Chebyshev and Fourier Spectral Methods, Dover Publications, Inc., 2nd edition, 2000.

[18] S. B. Zheng, A. J. Wootton, E. R. Solano, Analytical tokamak equilibrium for shaped plasmas, Phys. Plasmas 3 (1996) 1176–1178.

[19] A. J. Cerfon, J. P. Freidberg, "one size fits all" analytic solutions to the grad–shafranov equation, Phys. Plasmas 17 (2010) 032502.

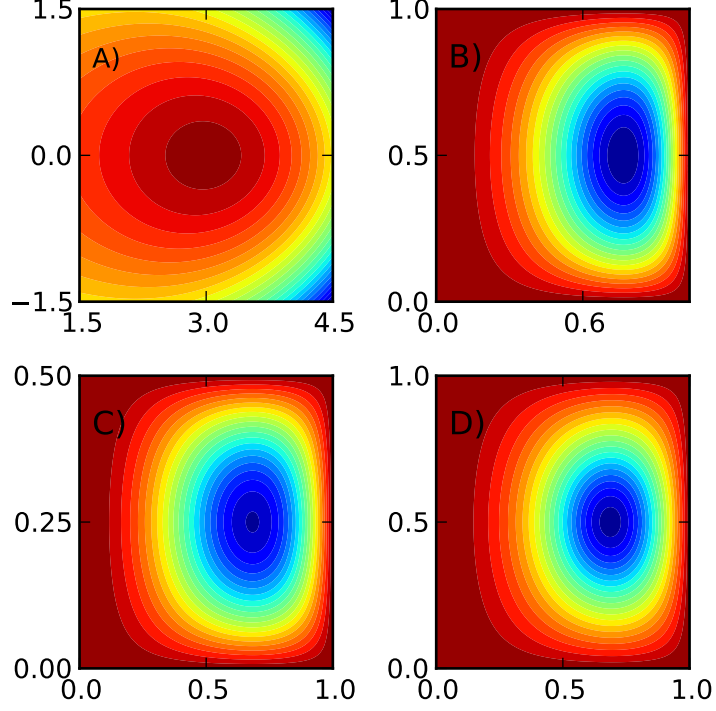[20] G. Strang, G. J. Fix, An Analysis of the Finite Element Method, Prentice-Hall, 1973.

Figure 1: Equilibrium poloidal flux contours for the A) Solev'ev equilibrium, B) FRC equilibrium, C) spheromak equilibrium, and D) nonlinear equilibrium.

Equilibria	F model	P model
Solev'ev	$FF' = S_2$	$P = -S_1\psi + P_0$
FRC	$F = 0$	$P = P_0 + P_2(1 - \hat{\psi}^2)$
Spheromak	$F = f_1(1 - \hat{\psi})$	$P = P_0$
Nonlinear	$F = (1 - \hat{\psi}) + \hat{\psi}(\hat{\psi} - 1)/4$	$P = P_a(1 - 3\hat{\psi}^2 + 2\hat{\psi}^3)$, and $P = P_a$

Table 1: A summary of the pressure and toroidal field models used for each of equilibria.

Polynomial degree	Solev'ev	FRC	Spheromak
2	-3.8	-3.5	-3.9
3	-4.9	-4.5	-4.9
4	-5.5	-5.2	-6.0

Table 2: Algebraic rates of convergence of ψ for the Solev'ev, FRC, and Spheromak equilibria.
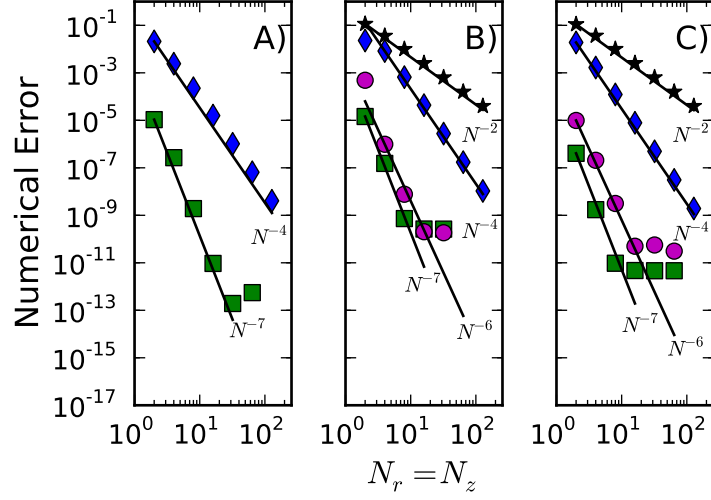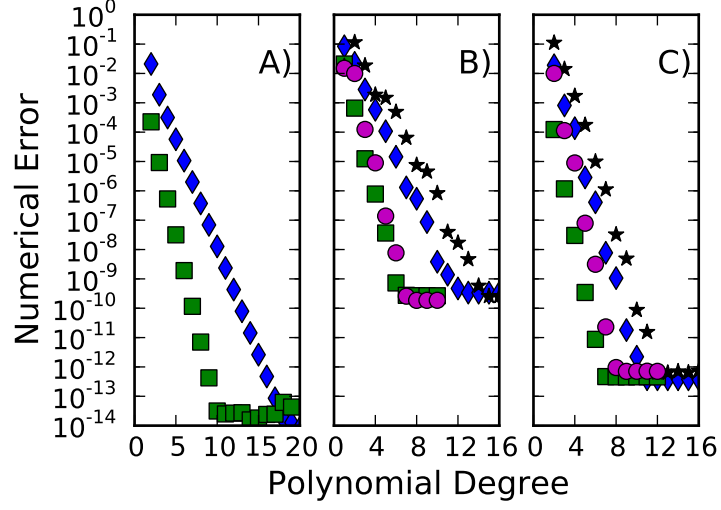
Figure 2: H-refinement convergence studies for the A)Solev'ev equilibrium, B)FRC equilibrium, and C) spheromak equilibrium. The numerical error in ψ is plotted for 2nd order elements ($\blacklozenge$) and 6th order elements ($\blacksquare$). The numerical error in B_r is also plotted for the FRC and spheromak equilibria for polynomials of degree 2 ($\star$) and polynomials of degree 6 ($\bullet$). Reference lines are added showing indicated rates of convergence.

Polynomial degree	FRC	Spheromak
2	-1.9	-1.9
3	-3.2	-3.2
4	-3.9	-3.9

Table 3: Algebraic rates of convergence of B_r for the FRC, and Spheromak equilibria.

16

Figure 3: P-refinement convergence studies for the A)Solev'ev equilibrium, B)FRC equilibrium, and C) spheromak equilibrium. The numerical error in ψ is plotted for a 2x2 ($\blacklozenge$) and 8x8 ($\blacksquare$) element mesh. The numerical error in B_r is also plotted for the FRC and spheromak equilibria for the 2x2 mesh ($\star$) and 8x8 ($\bullet$) element mesh.
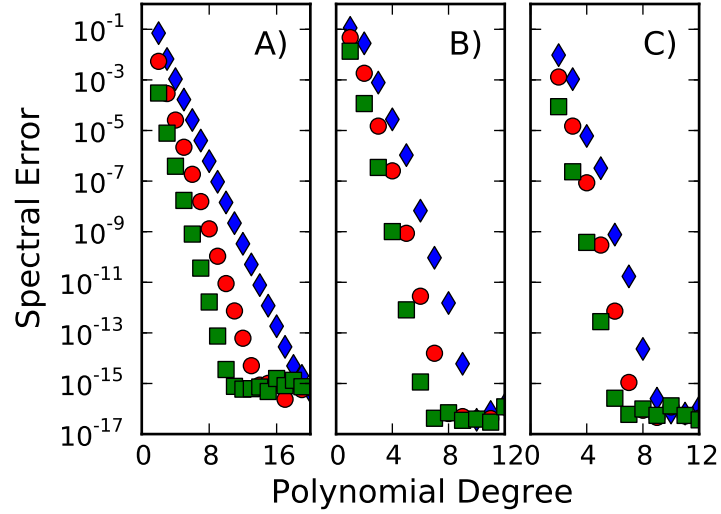

Figure 4: Spectral error in ψ for the A)Solev'ev equilibrium, B)FRC equilibrium, and C) spheromak equilibrium for a 2x2 ($\blacklozenge$), 4x4 ($\bullet$), and 8x8 ($\blacksquare$) element mesh.
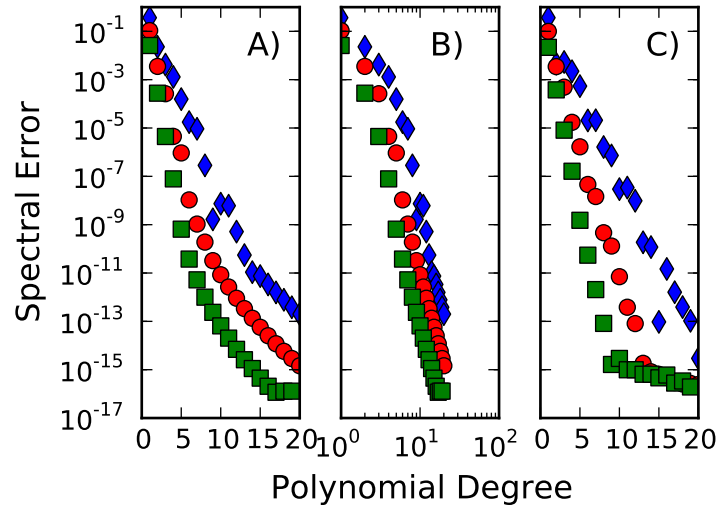
17

Figure 5: Spectral error in ψ for the nonlinear equilibrium with a cubic pressure profile on a A)log-linear plot, B) a log-log plot, and C) the error with a constant pressure profile on a log-linear plot for a 2x2 (♦), 4x4 (●), and 8x8 (■) element mesh.